Journal of Alloys and Compounds, 213/214 (1994) 43–49
JALCOM 4061

Applications of a global nuclear structure model to studies of the heaviest elements

Peter Möller and J. Rayford Nix
Theoretical Division, Los Alamos National Laboratory, Los Alamos, NM 87545 (USA)

Abstract

We present some new results on heavy element nuclear structure properties calculated on the basis of the finite-range droplet model and folded Yukawa single-particle potential. Specifically, we discuss calculations of nuclear ground state masses and microscopic corrections, α decay properties, β decay properties, fission potential energy surfaces, and spontaneous fission half-lives. These results, obtained with a global nuclear structure approach, are particularly reliable for describing the stability properties of the heaviest elements.

1. Introduction

The number of elements is limited, because nuclei become increasingly unstable with respect to spontaneous fission and α decay as the proton number increases. As early as the mid-1960s, it was speculated that this trend might be broken at the next magic numbers beyond those in the doubly magic nucleus $^{208}_{82}Pb_{126}$. Many calculations on the properties of the heaviest elements were carried out over the next several years. However, since that time, significant improvements have been incorporated into the model that we use for these studies, and we present here some of our most recent results. More extensive presentations will appear in a forthcoming review [1] and in a forthcoming issue of *Atomic Data and Nuclear Data Tables* [2]. The new results are particularly reliable in the heavy element region.

2. Model

In the macroscopic–microscopic method, the total potential energy, calculated as a function of the shape, proton number Z and neutron number N, is the sum of a macroscopic term and a microscopic term, representing the shell-plus-pairing correction. Thus, the total nuclear potential energy can be written as

$$E_{\rm pot}(Z,N,\text{ shape}) = E_{\rm mac}(Z,N,\text{ shape}) + E_{\rm s+p}(Z,N,\text{ shape}) \quad (1)$$

The preferred model in the current calculations has its origin in a 1981 nuclear mass model [3, 4] which utilized the folded Yukawa single-particle potential developed in 1972 [5, 6]. The macroscopic model used in the 1981 calculation was a finite-range, liquid-drop model which contained a modified surface energy term to account for the finite range of the nuclear force. The modified surface energy term was given by the Yukawa-plus-exponential finite-range model [7]. This model is used in our calculation of fission potential energy surfaces.

Our preferred macroscopic model is now the finite-range droplet model, for which additions of finite range surface energy effects and an exponential term [8] have resulted in dramatic improvements in its predictive properties, as summarized in the discussion of Table A in ref. 9. We refer to this new macroscopic model as the finite-range droplet model (FRDM; this abbreviation is also used to designate the full macroscopic–microscopic nuclear structure model). For the calculation of the ground state properties, we use here the latest version, which is denoted FRDM(1992) [2].

3. Ground state properties

Figure 1 shows the results of the FRDM(1992) nuclear mass calculation. The discrepancy between the measured and calculated masses shown in the lower part of the figure is quite small, particularly in the heavy region. The good agreement results from several essential new features in the calculation relative to those in the 1981 calculation [3, 4], namely a new macroscopic model, a Lipkin–Nogami pairing model with an improved form and parameters of the effective-interaction pairing gap [10], and minimization of the ground state energy

Elsevier Science S.A.
SSDI 0925-8388(94)04061-8

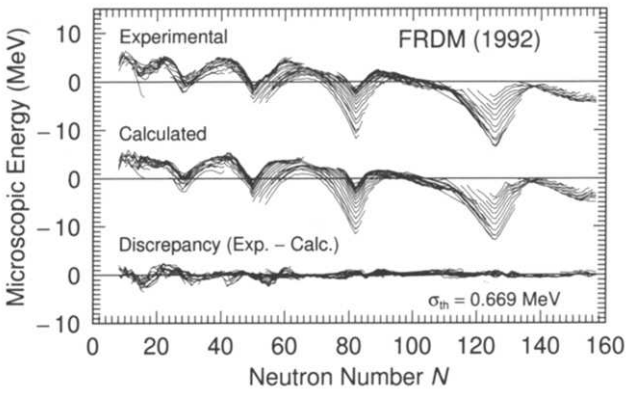

Fig. 1. Comparison of experimental and calculated microscopic corrections for 1654 nuclei, for a macroscopic model corresponding to the FRDM (1992). The bottom part showing the difference between these two quantities is equivalent to the difference between the measured and calculated ground state masses. There are almost no systematic errors remaining for nuclei above $N = 65$, for which region the error is only 0.448 MeV.

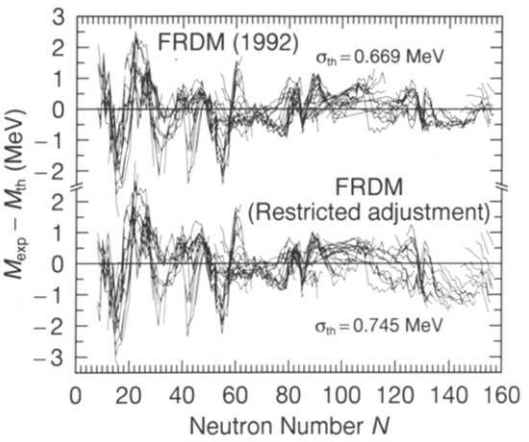

Fig. 2. Test of extrapolability of the FRDM towards the superheavy region. The top part of the figure shows the error of the standard FRDM. In the lower part, the error was obtained from a mass model whose constants were determined from adjustments to the restricted set of nuclei with $Z, N \geqslant 28$ and $A \leqslant 208$. In the heavy region, there is some increase in the spread of the error but no systematic divergence of the mean error.

with respect to higher multipole shape distortions [11]. The FRDM accounts for Coulomb redistribution effects, which are particularly important in the heavy region [11]. To ensure the reliability of a nuclear mass model for extrapolation to the superheavy region, it is necessary, in our opinion, to use a global approach in which the model constants are adjusted to a large region of the periodic system, as is done here. Approaches in which the model constants are adjusted to a limited heavy region, such as the region above Pb, are much less reliable for extrapolation into the superheavy region.

To test the reliability of the FRDM for extrapolation beyond the heaviest known elements, we performed a rather severe test in which we adjusted the model constants only to data in the region $Z, N \geqslant 28$ and $Z \leqslant 208$. There are 1110 known masses in this region, compared with 1654 in the region $Z, N \geqslant 8$ used in our standard adjustment. Thus, about one-third of all known masses are excluded, with nuclei removed from both ends of the region of adjustment. We then applied the model with these constants to the calculation of all known masses in our standard region and compare the results with our standard model in Fig. 2. The error for the known nuclei is now 0.745 MeV, compared with 0.669 MeV in our standard model adjusted to all known nuclei. Although there is a noticeable increase in the error in the regions that were not included in the adjustment, an inspection of Fig. 2 indicates that the increased error in the heavy region does not result from a systematic divergence of the mean error but rather from a somewhat larger scatter in the error.

In our standard model, the mass excesses of $^{272}110$ and $^{288}110$ are 133.82 MeV and 165.68 MeV respectively. In our restricted adjustment, we obtain 133.65 MeV and 166.79 MeV respectively. Thus, although $^{288}110$ is 80 units in A away from the last nucleus included in the restricted adjustment, the mass obtained in this numerical experiment is only about 1 MeV different from that obtained in the calculation whose constants were adjusted to nuclei up to 50 units in A closer to the superheavy region. Since our standard calculation is adjusted so much closer to the superheavy region than is the numerical experiment, we feel that it should be accurate to about 1 MeV in the superheavy region.

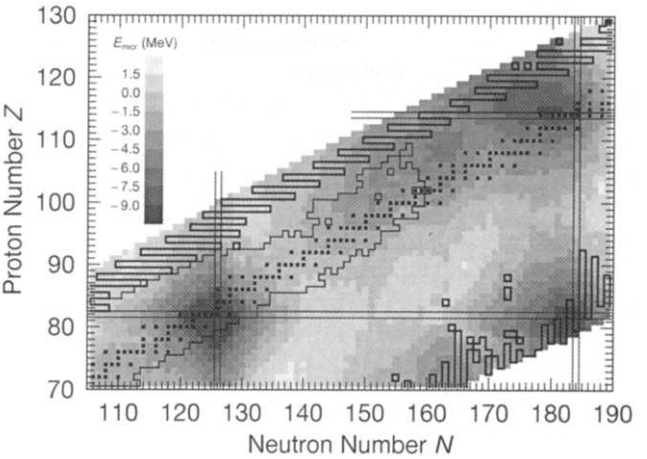

Fig. 3. Contour diagram of calculated microscopic corrections at the end of the periodic system. Solid squares indicate nuclei that are calculated to be stable with respect to β decay. The well-known doubly magic nucleus $^{208}_{82}Pb_{126}$ is associated with the minimum in the shell correction in the lower left-hand corner. Superheavy nuclei are associated with the minimum in the upper right-hand corner.

In Fig. 3, we show that calculated microscopic corrections for heavy nuclei, with nuclei that are calculated to be β stable shown as solid squares. The region of known nuclei is bordered by a thin solid line. The

proton and neutron drip lines, where the corresponding separation energies are zero, are shown by thick solid lines located near the left- and right-hand edges of the shaded region respectively. Minima in contour diagrams of calculated microscopic corrections are usually associated with pairs of magic neutron and proton numbers. Thus, in the lower left-hand corner of the diagram, we see a minimum below -10 MeV, corresponding to the doubly magic nucleus $^{208}_{82}Pb_{126}$. In the upper right-hand corner of the figure is another minimum at proton number $Z=115$ and neutron number $N=179$, at an energy of -9.44 MeV. At $Z=114$ and $N=179$, the energy is almost the same. This minimum is located in the region of superheavy elements. An interesting feature of the contour diagram is that there is a peninsula of stability, extending from the superheavy island toward the region of known heavy elements. On this peninsula, there is a "rock" of increased stability centered at $Z=109$ and $N=163$.

The three heaviest known elements $_{107}$Ns, $_{108}$Hs and $_{109}$Mt were all identified from their α decay chains [12–14], which limited their stability. The single most important quantity determining the α decay half-life is the Q value of the decay. In the heavy element region, an uncertainty of 1 MeV in the Q value corresponds to uncertainties of $10^{\pm 5}$ and $10^{\pm 3}$ for $Q_\alpha \approx 7$ MeV and $Q_\alpha \approx 9$ MeV respectively [15].

In 1989 Münzenberg *et al* [16] compared Q values for α decay along the $N=154$ and $N=155$ isotonic lines with predictions of the 1988 FRDM [17]. In Fig. 4, we make a similar comparison of measured data with predictions of the current FRDM [2]. These results based on the current FRDM show a much improved agreement with the measured values relative to the comparison with the earlier mass model of Münzenberg *et al.* [16].

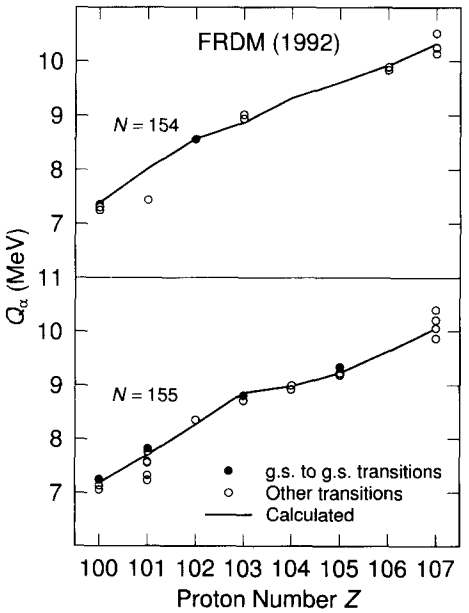

Fig. 4. Comparison of measured and calculated α decay Q values for the $N=154$ and 155 isotonic chains.

We estimated α decay half-lives T_α corresponding to our calculated Q_α values by using the Viola–Seaborg systematics [18] with parameter values that were determined in an adjustment that included new data for even–even nuclei [19]. The nucleus $^{272}110$ has a calculated α decay half-life of about 70 ms. The nuclei $^{288}110$ and $^{290}110$ in the center of the superheavy island have calculated α decay half-lives of 4 years and 1565 years respectively. If accurate, this rules out the possibility that superheavy elements occur in nature.

Applications of our model to the calculation of β decay half-lives and β-delayed neutron emission are discussed elsewhere [20, 21].

4. Fission properties

For a long time, experimental studies of spontaneous fission properties showed gradual, predictable changes of such properties as spontaneous fission half-lives and mass and kinetic energy distributions as the region of known nuclei above uranium expanded. However, in the 1970s, evidence started to accumulate that there were rapid changes in the fission properties in the heavy Fm region. The first observation of the onset of symmetric fission at the end of the periodic system was a study [22] of ^{257}Fm fission.

For ^{258}Fm, the changes are even more dramatic. Fission becomes symmetric, with a very narrow mass distribution; the kinetic energy of the fragments is about 35 MeV higher than that in the asymmetric fission of ^{256}Fm; and the spontaneous fission half-life is 0.38 ms compared with 2.86 h for ^{256}Fm. The fission fragment mass distributions and kinetic energy distributions of ^{258}Fm and four other heavy nuclei are shown in Fig. 5, taken from ref. 23.

An important feature of some of the kinetic energy distributions is that the shape is not Gaussian. Instead, some of the distributions are best described as a sum of two Gaussians. For ^{258}Fm, for example, the kinetic energy distribution can be represented by two Gaussians centered at about 200 and 235 MeV. This type of fission is referred to as "bimodal" fission.

It has been proposed that the rapid change in half-life when going from ^{256}Fm to ^{258}Fm results from the disappearance of the second saddle in the barrier below the ground state energy. Fission through only one barrier, the first, gives very good agreement with the observed short half-life of ^{258}Fm [24, 25]. However, one may ask if and how the spontaneous fission half-life is connected to the change in other fission properties at this transition point, such as the change to symmetric

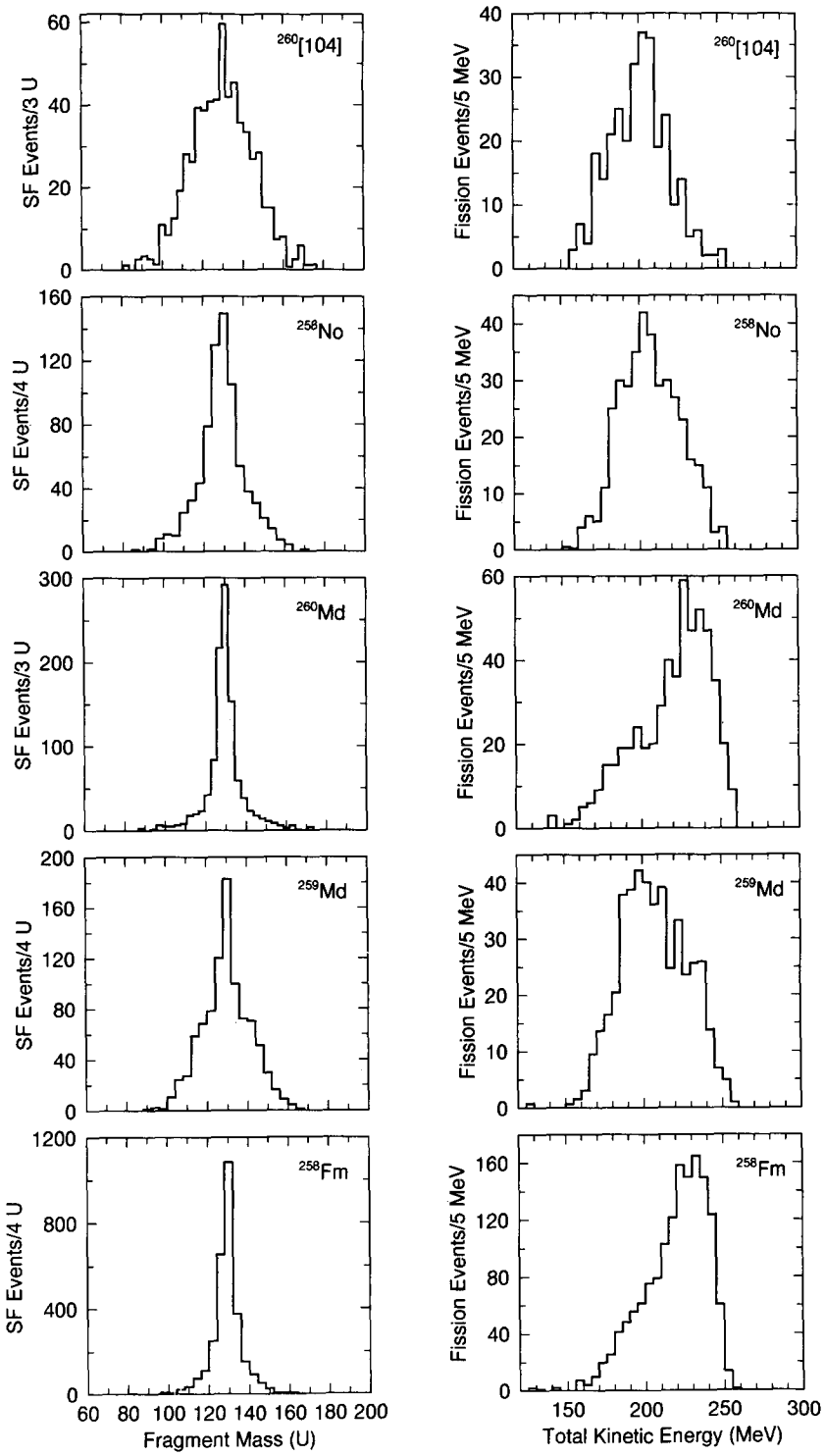

Fig. 5. Experimental fission fragment mass and kinetic energy distributions for the fission of nuclei close to ^{264}Fm, whose symmetric fragments are doubly magic. The structures of these distributions reflect the valleys, ridges, minima and saddle-points of the underlying nuclear potential energy surfaces.

fission and high kinetic energies. We have shown that the old interpretation, that the barrier of ^{258}Fm has disappeared below the ground state, is inconsistent with results from the present calculation, and propose a new mechanism for the short half-life.

Although theoretical considerations had far earlier led to suggestions of several fission paths in the potential energy surface, theoretical spontaneous fission half-life calculations until rather recently considered only shape parameterizations that allowed for the conventional

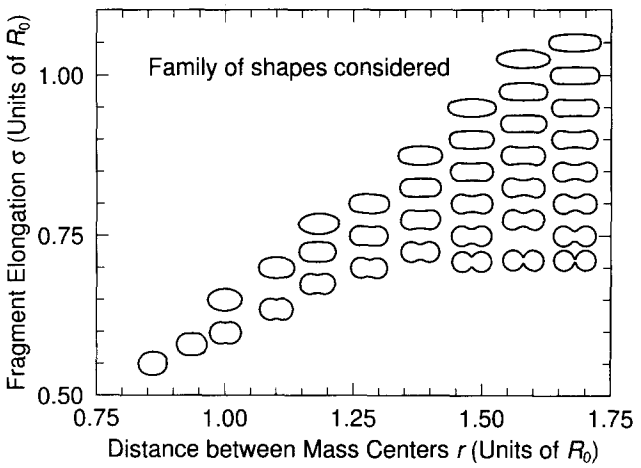

Fig. 6. Nuclear shapes for which fission potential energy surfaces are calculated. The selected shapes allow fission into both compact spherical fragments with high kinetic energies and elongated fragments with normal kinetic energies.

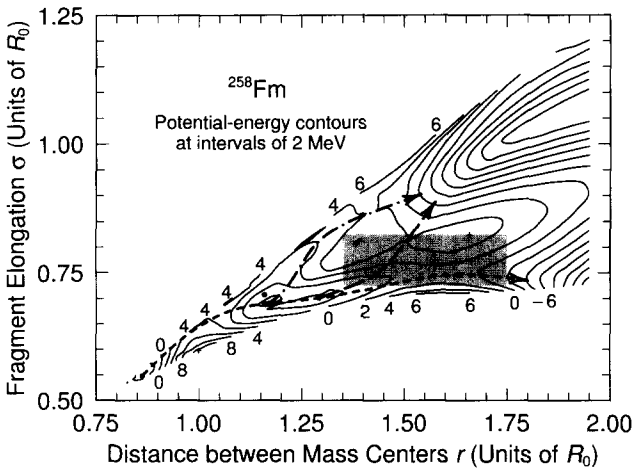

Fig. 7. Calculated potential energy surface for ^{258}Fm at intervals of 2 MeV, showing three paths to fission. Initially, only one path starting at the ground state exists. Later, this path divides into two paths, one leading to compact scission shapes in the lower part of the figure and the other leading to elongated shapes in the upper part of the figure. At a late stage in the barrier-penetration process, a third "switchback path" branches off from the path leading to compact shapes, and leads back into the valley of elongated scission shapes. Because this takes place late in the barrier-penetration process, the fission probabilities for fission into compact and elongated shapes are expected to be roughly comparable. Experimentally, the probabilities differ by only one order of magnitude. The inertia associated with fission into the lower valley is considerably smaller than the inertia for fission into the upper valley.

valleys [6, 26–30]. Early calculations that showed, to some extent, the effect of fragment shells at a relatively early stage of the fission process (before scission) appeared in the early to mid-1970s [31–33]. The first calculation that showed a pronounced multivalley structure and predicted the corresponding spontaneous fission half-lives was performed in refs. 34, 35. An improved model that also included odd nuclei was presented somewhat later [36]. We show results from these calculations in Figs. 6–10, in units where the radius R_0 of the spherical nucleus is unity. These results [34, 36] showed that some of the good agreement between the calculated spontaneous fission half-lives and measured values obtained in earlier calculations [25, 27] for nuclei close to ^{258}Fm was fortuitous.

The high kinetic energy fragments in heavy Fm fission were thought to correspond to fission through a scission configuration of two touching spherical fragments, while low kinetic energy fission was interpreted as fission through a scission configuration of two elongated fragments. Figure 6 shows a set of shapes that leads from

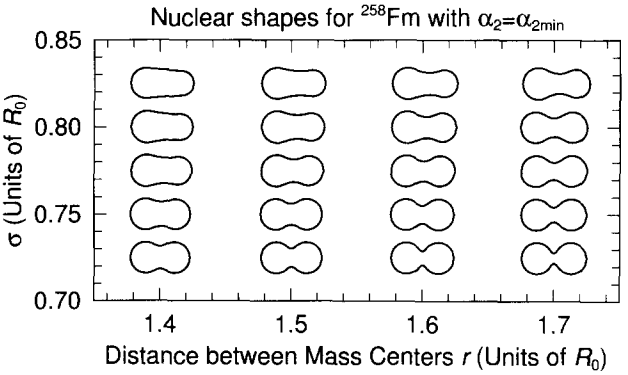

Fig. 8. Shapes corresponding to the contour map in Fig. 9. Shapes associated with the new valley are in the lower part of the figure and remain symmetric. As the switchback path from the new valley crosses over the saddle at $r=1.4$ and $\sigma=0.75$ into the old valley, asymmetry becomes increasingly more pronounced. As asymmetry develops, the overall extension of the nucleus remains approximately constant for fixed values of r.

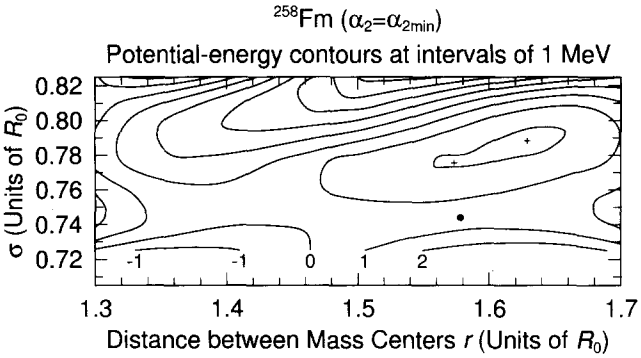

Fig. 9. Contour map for ^{258}Fm, showing the vicinity of the outer saddle along the new valley and the saddle along the switchback path between the new valley and the old valley. The energy has been minimized with respect to the mass asymmetry coordinate α_2 for fixed values of the other symmetric three quadratic surface shape parameters. The new valley enters in the extreme lower left-hand corner of this figure, and fission may either evolve into the old valley across the saddle at $r=1.4$ and $\sigma=0.75$ or proceed in the direction of compact scission shapes across the saddle at $r=1.6$ and $\sigma=0.74$. These two saddles are of about equal height.

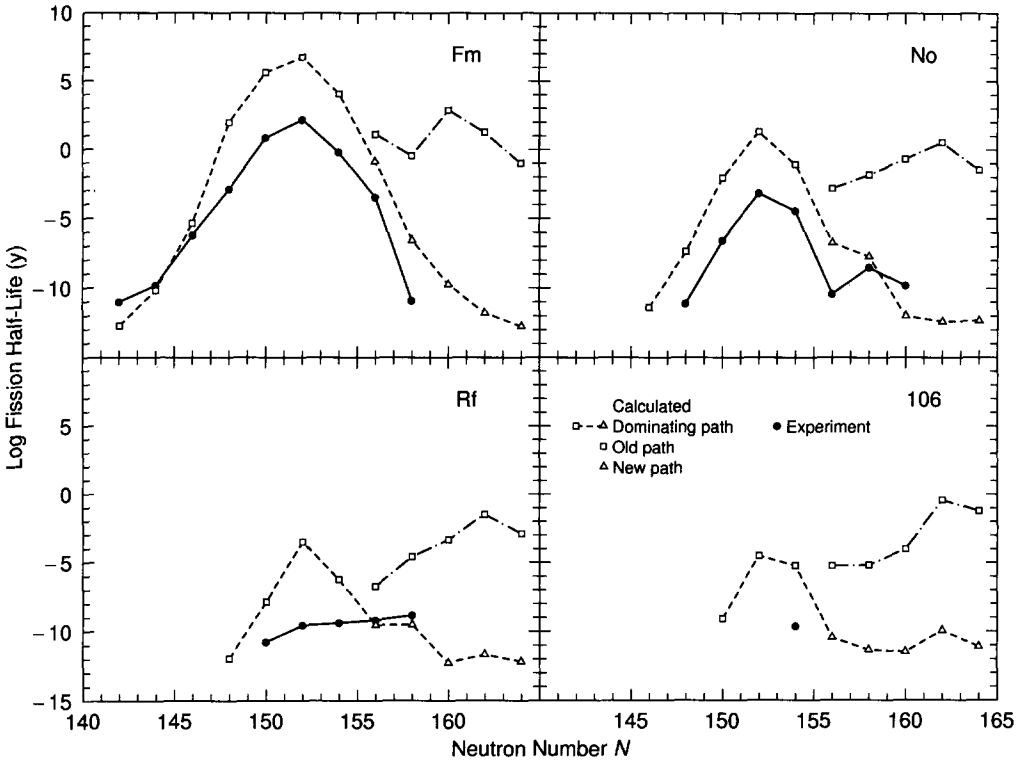

Fig. 10. Experimental spontaneous fission half-lives compared with calculated values for fission along the old and new valleys. A new valley is present in the calculated potential energy surface only for $N \geqslant 158$. When half-lives have been calculated for both valleys for a particular neutron number, the shorter (dominating) calculated half-lives should be compared with experimental values. The discrepancy between calculated and experimental values in the vicinity of $N=152$ may arise from an error in the calculated ground state energy or the neglect of fission along the third (switchback) path. For No, there is a new experimental feature of fairly constant half-life for $N \gtrsim 156$, which is reproduced moderately well by the calculations. For Rf, the experimental half-life is nearly constant as a function of N. The theoretical half-lives for Rf are too high near $N=152$. However, the discrepancy corresponds only to an error of about 1 MeV in the calculated ground state energy. For $Z=106$, the calculated half-life in the new valley is fairly constant beyond $N=156$. This shows that the destabilizing effect of the spherical magic fragment neutron number $Z=2\times82$ approximately cancels the effect of the deformed magic ground state neutron number $N=162$.

a deformed ground state to both these scission configurations, and Fig. 7 shows the corresponding calculated potential energy surface. The three paths are discussed in the caption to Fig. 7.

In the shaded region of Fig. 7, we have investigated the effect of a third mass-asymmetric deformation. The resulting most favorable shapes are shown in Fig. 8, with the potential energy corresponding to these shapes shown in Fig. 9. The saddle along the long-dashed switchback path has been lowered by mass asymmetry, but the saddle leading to two touching spherical fragments is not lowered by this mass asymmetry. The reason that this saddle appears somewhat higher in Fig. 7 than that in Fig. 9 is a result of interpolation difficulties in a region of rapidly changing energy in Fig. 7.

Finally, we present in Fig. 10 the calculated and measured spontaneous fission half-lives for some heavy elements of interest. Spontaneous fission half-lives are related to an integral along the fission path of the product of an inertia function and the barrier along the fission path. Because the barrier in the valley leading to two touching spheres is calculated to be above the ground state energy for ^{258}Fm, the mechanism of the short half-life is not the absence of a second peak in the barrier. Instead, it is a very low inertia associated with fission in the new valley. No truly reliable microscopic calculation of the inertia along different fission paths exists at present, but the level structure in the new valley suggests a very low inertia for fission along this path.

5. Summarizing remarks

We conclude by summarizing some important results on the stability of the heaviest elements presented here.

(1) The inclusion of Coulomb redistribution effects in the mass model lowers the calculated mass for ^{272}110 by about 3 MeV.

(2) The superheavy island is now predicted to be centered around ^{288}110 and ^{290}110.

(3) The calculated α decay half-lives of $^{272}110$, $^{288}110$ and $^{290}110$ are 70 ms, 4 years and 1565 years respectively.

(4) Relative to earlier results, we obtained shorter spontaneous fission half-lives in the super heavy region. For nuclei in the vicinity of $^{272}110$, a "ballpark" value is 1 ms. Thus, some spontaneous fission half-lives may be comparable with α decay half-lives.

(5) Spontaneous fission half-lives may be significantly different from the "ballpark" value of 1 ms for two reasons. One reason is the general uncertainty of the calculations. Another reasons is that, for odd systems, specialization energies can lead to huge increases in spontaneous fission half-lives, with up to 10 orders of magnitude possible.

More extensive discussions of the results presented here may be found in a series of recent publications [1, 2, 10, 11, 20, 34, 36, 37].

Acknowledgment

This work was supported by the US Department of Energy.

References

1 P. Möller and J.R Nix, *J. Phys. G,* in press.
2 P. Möller, J.R. Nix, W.D. Myers and W.J. Swiatecki, *Atom. Data Nucl. Data Tables*, in press.
3 P. Möller and J.R. Nix, *Nucl. Phys. A, 361* (1981) 117.
4 P. Möller and J.R. Nix, *Atom. Data Nucl. Data Tables, 26* (1981) 165.
5 M. Bolsterli, E.O. Fiset, J.R. Nix and J.L. Norton, *Phys. Rev. C, 5* (1972) 1050.
6 P. Möller and J.R. Nix, *Nucl. Phys. A, 229* (1974) 269.
7 H.J. Krappe, J.R. Nix and A.J. Sierk, *Phys. Rev. C, 20* (1979) 992.
8 P. Möller, W.D. Myers, W.J. Swiatecki and J. Treiner, *Proc. 7th Int. Conf. on Nuclear Masses and Fundamental Constants, Darmstadt-Seeheim, 1984*, Lehrdruckerei, Darmstadt, 1984, p. 457.
9 P. Möller, W.D. Myers, W.J. Swiatecki and J. Treiner, *Atom. Data Nucl. Data Tables, 39* (1988) 225.
10 P. Möller and J.R. Nix, *Nucl. Phys. A, 536* (1992) 20.
11 P. Möller, J.R. Nix, W.D. Myers and W.J. Swiatecki, *Nucl. Phys. A, 536* (1992) 61.
12 G. Münzenberg, S. Hofmann, F.P. Hessberger, W. Reisdorf, K.-H. Schmidt, J.R.H. Schneider, P. Armbruster, C.-C. Sahm and B. Thuma, *Z. Phys. A, 300* (1981) 7.
13 G. Münzenberg, P. Armbruster, F.P. Hessberger, S. Hofmann, K. Poppensieker, W. Reisdorf, J.R.H. Schneider, W.F.W. Schneider, K.-H. Schmidt, C.-C. Sahm and D. Vermeulen, *Z. Phys. A, 309* (1982) 89.
14 G. Münzenberg, P. Armbruster, H. Folger, F.P. Hessberger, S. Hofmann, J. Keller, K. Poppensieker, W. Reisdorf, K.-H. Schmidt, H.J. Schött, M.E. Leino and R. Hingmann, *Z. Phys. A, 317* (1984) 235.
15 E.O. Fiset and J.R. Nix, *Nucl. Phys. A, 193* (1972) 647.
16 G. Münzenberg, P. Armbruster, S. Hofmann, F.P. Hessberger, H. Folger, J.G. Keller, V. Ninov, K. Poppensieker, A.B. Quint, W. Reisdorf, K.-H. Schmidt, J.R.H. Schneider, H.J. Schött, K. Sümmerer, I. Zychor, M.E. Leino, D. Ackermann, U. Gollerthan, E. Hanelt, W. Morawek, D. Vermeulen, Y. Fujita and T. Schwab, *Z. Phys. A, 333* (1989) 163.
17 P. Möller and J.R. Nix, *Atom. Data Nucl. Data Tables, 39* (1988) 213.
18 V.E. Viola, Jr., and G.T. Seaborg, *J. Inorg. Nucl. Chem., 28* (1966) 741.
19 A. Sobiczewski, Z. Patyk and S. Ćwiok, *Phys. Lett. B, 224* (1989) 1.
20 P. Möller and J. Randrup, *Nucl. Phys. A, 514* (1990) 1.
21 K.-L. Kratz, J.-P. Bitouzet, F.-K. Tielemann, P. Möller and B. Pfeiffer, *Ap. J., 403* (1993) 216.
22 J.P. Balagna, G.P. Ford, D.C. Hoffman, and J.D. Knight, *Phys. Rev. Lett., 26* (1971) 145.
23 E.K. Hulet, J.F. Wild, R.J. Dougan, R.W. Lougheed, J.H. Landrum, A.D. Dougan, M. Schädel, R.L. Hahn, P.A. Baisden, C.M. Henderson, R.J. Dupzyk, K. Sümmerer and G.R. Bethune, *Phys. Rev. Lett., 56* (1986) 313.
24 J. Randrup, C.F. Tsang, P. Möller, S.G. Nilsson and S.E. Larsson, *Nucl. Phys. A, 217* (1973) 221.
25 J. Randrup, S.E. Larsson, P. Möller, S.G. Nilsson, K. Pomorski and A. Sobiczewski, *Phys. Rev. C, 13* (1976) 229.
26 P. Möller, *Nucl. Phys. A, 192* (1972) 529.
27 A. Baran, K. Pomorski, A. Łukasiak and A. Sobiczewski, *Nucl. Phys. A, 361* (1981) 83.
28 G.A. Leander, P. Möller, J.R. Nix and W.M. Howard, *Proc. 7th Int. Conf. on Nuclear Masses and Fundamental Constants, Darmstadt-Seeheim, 1984*, Lehrdruckerei, Darmstadt, 1984, p. 466.
29 K. Böning, Z. Patyk, A. Sobiczewski and S. Ćwiok, *Z. Phys. A, 325* (1986) 479.
30 A. Staszczak, S. Pilat and K. Pomorski, *Nucl. Phys. A, 504* (1989) 589.
31 U. Mosel and H.W. Schmitt, *Phys. Rev. C, 4* (1971) 2185.
32 A. Šandulescu, R.K. Gupta, W. Scheid and W. Greiner, *Phys. Lett. B, 60* (1976) 225.
33 P. Möller and J.R. Nix, *Nucl. Phys. A, 281* (1977) 354.
34 P. Möller, J.R. Nix and W.J. Swiatecki, *Nucl. Phys. A, 469* (1987) 1.
35 P. Möller, J.R. Nix and W.J. Swiatecki, *Proc. Int. School-Seminar on Heavy Ion Physics, Dubna, USSR, 1986, JINR Rep. JINR-D7-87-68*, 1987, p. 167.
36 P. Möller, J.R. Nix and W.J. Swiatecki, *Nucl. Phys. A, 492* (1989) 349.
37 P. Möller, J.R. Nix, K.-L. Kratz, A. Wöhr and F.-K. Thielemann, *Proc. 1st Symp. on Nuclear Physics in the Universe, Oak Ridge, TN, 1992,* Institute of Physics, Bristol, 1993, p.433.